A Motion-Tolerant Adaptive Algorithm for Wearable Photoplethysmographic Biosensors

Rasoul Yousefi, *Student Member, IEEE*, Mehrdad Nourani, *Senior Member, IEEE*, Sarah Ostadabbas, *Student Member, IEEE*, and Issa Panahi, *Senior Member, IEEE*

***Abstract*—The performance of portable and wearable biosensors is highly influenced by motion artifact. In this paper, a novel real-time adaptive algorithm is proposed for accurate motion-tolerant extraction of heart rate (HR) and pulse oximeter oxygen saturation (SpO_2) from wearable photoplethysmographic (PPG) biosensors. The proposed algorithm removes motion artifact due to various sources including tissue effect and venous blood changes during body movements and provides noise-free PPG waveforms for further feature extraction. A two-stage normalized least mean square adaptive noise canceler is designed and validated using a novel synthetic reference signal at each stage. Evaluation of the proposed algorithm is done by Bland–Altman agreement and correlation analyses against reference HR from commercial ECG and SpO_2 sensors during standing, walking, and running at different conditions for a single- and multisubject scenarios. Experimental results indicate high agreement and high correlation (more than 0.98 for HR and 0.7 for SpO_2 extraction) between measurements by reference sensors and our algorithm.**

***Index Terms*—Adaptive filter, motion artifact, noise reduction, photoplethysmography (PPG), pulse oximeter, wearable biosensor.**

I. Introduction

A. Motivation

PHOTOPLETHYSMOGRAPHY (PPG) is a noninvasive measurement of the blood flow at the surface of the skin by using red and infrared lights. Two common applications of the PPG are calculations of the arterial oxygen saturation and heart rate (HR). There are several new applications in different stages of maturity that require various analyses on the PPG signal including amplitude, rhythm, peripheral pulse, respiratory variability, and tissue perfusion. For example, increased and decreased signal amplitude can be signs of vasodilation and vasoconstriction, respectively [1]. The amplitude is directly proportional to the vascular distensibility [2]. PPG signals were also found to be useful for detection and diagnosis of cardiac arrhythmias [3], [4]. PPG signal is known to be sensitive to pulsatile blood flow and captures the peripheral pulses. The pressure at which the pulse is captured highly corresponds to the systolic blood pressure (BP) [5]. The respiratory rate can be reliably determined by PPG signal [6]–[8]. Noninvasive continuous tissue perfusion and peripheral blood flow detection is another potential advantage of the PPG signal.

All the aforementioned applications require a clean and enhanced signal for feature extraction, analysis, and monitoring. Therefore, the signal quality is critical for wearable PPG signals and systems [9], [10]. In new wearable and implantable devices/applications, the biometric signal needs to be monitored during daily activities where motion is always present. Motion artifact is the most problematic source of noise which deteriorates signal integrity and can, in the worst case, corrupt it to such an extent that it might be rendered clinically unusable. Examples from motions of the patient in real-world clinical setting are movement during transport, rubbing, waving, seizures, and kicking in neonates/infants. As a side effect, inaccurate reading and interpretation of the PPG signal due to motion artifact can increase caregiver's workload which can lead to an increased cost of care and inefficiency of patient's treatment [11]–[13]. Therefore, there is a high demand for an effective algorithm for wearable and mobile PPG biosensors to enhance the signal quality in the presence of motion artifact.

B. Current State of the Art

Despite all the attractive benefits and applications of the PPG signal and ease of integration into wearable devices, most of the useful information can be distorted or concealed by motion artifact. This is true in all wearable and portable applications in both clinical settings and daily activities. One of the commonly used methods to reduce artifact is adaptive noise cancellation using accelerometers as a noise reference signal [14], [15]. A 2-D active noise cancellation has been tried using the directional accelerometer data for finger PPG sensor [16]. The addition of a reflectance PPG sensor as the reference signal was implemented in [10]. Unfortunately, the reflectance PPG sensor is itself susceptible to motion. The main drawback of all these methods is the cost of extra hardware for the noise reference. Additionally, using three-axis accelerometer data is computationally intensive [10] and they truly reflect motion (as opposed to motion-induced noise). More precisely, researchers found no direct or high correlation between acceleration data from accelerometer and motion artifact in PPG signal [17]. To deal with this problem, a synthetic noise generation method is proposed using concurrent usage of singular value decomposition (SVD), independent component analysis (ICA), and fast Fourier transform (FFT) [18]. The algorithm basically assumes that the original PPG signal has only power at certain frequencies and the rest

Manuscript received October 23, 2012; revised January 8, 2013 and April 1, 2013; accepted May 13, 2013. Date of publication May 20, 2013; date of current version March 3, 2014.

The authors are with the Quality of Life Technology Laboratory, The University of Texas at Dallas, Richardson, TX 75080 USA (e-mail: r.yousefi@utdallas.edu; nourani@utdallas.edu; sarahostad@utdallas.edu; issa.panahi@utdallas.edu).

Color versions of one or more of the figures in this paper are available online at http://ieeexplore.ieee.org.

Digital Object Identifier 10.1109/JBHI.2013.2264358

is noise and then uses FFT, SVD, and ICA to generate three noise references. The algorithm switches between three generated reference noise signals by quantifying the randomness of each signal using skewness and kurtosis. Such assumption on motion artifact does not correlate well with different real-world sources of noise. Moreover, the highest randomness does not necessarily mean the highest correlation with the true motion artifact in the PPG signal.

On the industry side, Masimo Corporation has introduced discrete saturation transform (DST) to find pulse oximeter oxygen saturation in the presence of motion in portable devices [19], [20]. Typically, the DST algorithm consists of a reference signal generator, an adaptive filter, and a peak finder to find the most likely SpO_2 value based on the incoming signals. In this approach, the reference signal generator produces reference signals for all possible SpO_2 values. For each reference signal, the adaptive filter produces an output signal. Energy of each output signal is computed and plotted versus corresponding SpO_2 values. The right-most peak of the power plot (the largest saturation value) is nominally considered as oxygen saturation of arterial blood flow. Since this approach does not remove the motion artifact (e.g., due to tissue effect), the effect of motion artifact will be literally transformed to the output power plot in DST. More specifically, in presence of motion artifact, new peaks will be present on the output plot [21] and the peak finder may fail to find the peak corresponding to accurate SpO_2. Conversely, the peak corresponding to SpO_2 may be concealed due to high motion noise power causing the peak search to fail for that time window.

C. Main Contribution and Paper Organization

In order to address motion artifact issues and design a practical wearable PPG sensor, different sources of motion-induced error need to be identified, quantified, and estimated. In this paper, we enhance and expand our earlier work reported in [22] and use the basic optical theory of pulse oximetry to design and develop signal-processing techniques for noise reduction and signal enhancement. We propose a novel two-stage adaptive algorithm that efficiently removes the effect of tissue and venous blood noise during motion. This algorithm extracts fundamental period of the PPG signal, the HR, and the oxygen saturation level. The key contribution of our technique is to separate an extremely clean signal corresponding to the arterial blood flow. Once the clean signal is provided, a conventional technique can be used to extract the oxygen saturation value. In this paper, for experimentation, we have used the conventional *ratio of ratios* technique for SpO_2 extraction [23].

This paper is organized as follows. In Section II, a brief review of optical techniques of the PPG signal generation and optical theory behind the source of PPG signal are presented. In Section III, we quantify different noise components due to various sources and propose a reference noise generator. Then, we formulate the problem of optimum noise source generation to be used in the adaptive algorithm. The proposed algorithm is described in Section IV. The experimental setup and validation of the algorithm are in Section V and VI, respectively. The concluding remarks are in Section VII.

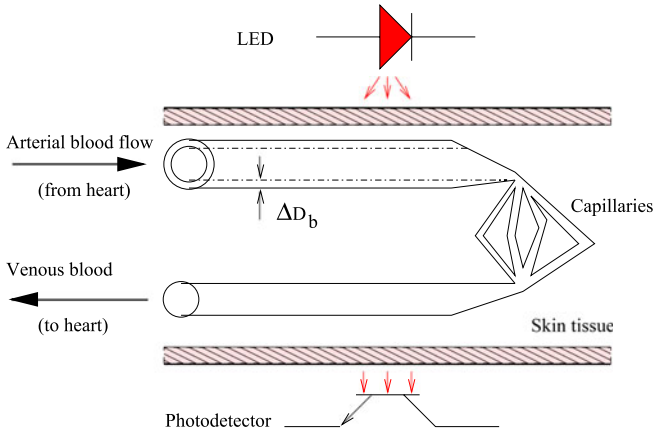

Fig. 1. Blood circulation.

II. Background

A. PPG Signal

A conventional pulse oximeter uses two small and easy to drive LED light sources with different wavelengths, i.e., a red LED and an infrared (IR) LED. A photodiode receiver captures the transmitted or reflected light sources. The analog front-end hardware uses a time-multiplexed approach with three phases: 1) activated red LED, 2) activated IR LED, and 3) dark phase. A transimpedance amplifier amplifies the current generated in photodiode due to optical density during active phases and provides a voltage signal. This signal will be filtered, amplified, and then sampled with an analog-to-digital converter for further processing.

The basic circulation of blood is conduced by heart, which pumps blood periodically and rhythmically into a branching system of arteries. The pulsations generated periodically will dampen by the time they reach the capillaries which are in contact with cells of tissues. As depicted in Fig. 1, the blood then returns in an almost steady stream to the heart with another pulsation stimulated in veins by muscular activity and the respiratory pump. An electronic interface captures these changes by an optical sensor on the site of measurement (e.g., finger) and provides the PPG signal with different components as shown in Fig. 2.

B. Theory of Optical Density

The source of the PPG signal is the optical density transmitted or reflected. As such, we will discuss and use optical theories developed for pulse oximetry. The basis of optical absorption is defined by Lambert–Beer's law [25] that explains the optical density (A) for both scatterer and nonscatterer as

$$A \stackrel{d}{=} \log\left(\frac{L_{\text{in}}}{L_{\text{out}}}\right) = E \cdot C \cdot D \tag{1}$$

where L_{in} and L_{out} are incident and transmitted light intensities, and C and D are the concentration and thickness of the

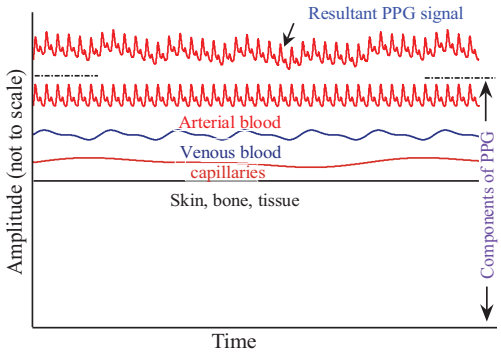

Fig. 2. Components of a typical PPG signal (from [24] with permission).

optical absorber, respectively. E is extinction coefficient which is intrinsic to the absorber and wavelength. The assumption in this formulation is that the object is uniform and nonscattering, so it only provides a rough estimation about scatterers. Two basic theories of optical scattering, which give us more precise prediction of scattering behaviors, are Rayleigh–Mie's theory and Schuster's theory [26]. Aoyagi who reported the principle of pulse oximetry in 1974 [27] has adopted the Schuster's theory and introduced the optical theory behind PPG. According to [26] and [27], the following relationship describes the optical density changes ΔA as a function of blood vessel thickness changes ΔD_b for a given blood vessel (see also Fig. 1):

$$\Delta A = [\sqrt{E_h(E_h + F)}Hb + Z_b]\Delta D_b \tag{2}$$

where $E_h \stackrel{d}{=} SE_o + (1-S)E_r$, in which E_o and E_r are the extinction coefficient of oxyhemoglobin and deoxyhemoglobin, respectively. S is oxygen saturation, Hb is hemoglobin concentrations of the blood, and F is the scattering coefficient. Z_b is a constant which becomes zero when the optical receiver is wide enough and independent of the working wavelength.

Tissue effect is reported to be one of the main sources of error in obtained optical density leading to undesired fluctuation in acquired PPG signal [26], [27]. Considering the effect of tissues, (2) is modified by adding a new term ($Z_t\ \Delta D_t$) and becomes

$$\Delta A = \sqrt{E_h(E_h + F)}Hb\ \Delta D_b + Z_b\Delta D_b + Z_t\ \Delta D_t \tag{3}$$

where Z_t is approximated to be a constant independent of the wavelength and ΔD_t is the thickness change of the tissue. Therefore, there is an optical density change (e.g., $Z_b\Delta D_b + Z_t\ \Delta D_t$) which is wavelength independent.

Equation (3) considers only one blood vessel. Considering the effect of both arterial and venous blood vessels, there are both arterial and venous blood changes. Therefore, ΔA is expressed as

$$\Delta A = \sqrt{E_a(E_a + F)}Hb_a\ \Delta D_a + \sqrt{E_v(E_v + F)}Hb_v\ \Delta D_v + \Delta A_s. \tag{4}$$

Subscripts a and v refer to arterial blood and venous blood, respectively. ΔD_v and ΔD_a are venous and arterial blood thickness changes, respectively [26], [27]. ΔA_s is independent of wavelength and it captures the accumulated wavelength-independent effect of both blood and tissue thickness changes. Using this experimentally validated theory of operation, we will present a noise removal technique in the next two sections.

III. Characterization and Formulation of Motion Artifact

In this section, first we formulate optical density to define a reference signal and a reference noise for removal of tissue effect and venous effect, respectively. Then, we model the arterial signal and define a cost function to find the optimum noise reference for removal of venous effect over time.

A. Effect of Tissue

When the body remains still, ΔD_t is close to zero and the effect of tissue manifests itself as a dc component in the recorded PPG signal, as shown in Fig. 2. This dc component can be removed in analog front-end or by digital filtering. However, in the presence of motion, this component is no longer constant. Fluctuations caused by body movements, for example, during walking, running, and treadmill exercise, can be clearly seen in the recorded PPG signal. Such new rhythmic pattern and variation in PPG signal can lead to an inaccurate and unreliable fundamental period for PPG signal. To deal with these issues, we employ two wavelengths to cancel out the effects of Z_t and Z_b that are independent of the wavelength [26], [27]. More specifically, we subtract optical densities [see (4)] corresponding to two-wavelength PPG biosensor (subscript i and j are used for wavelengths and t to represent tissue effect) and define the result by

$$\Delta A_{ij\_t} = [\sqrt{E_{a_i}(E_{a_i} + F)} - \sqrt{E_{a_j}(E_{a_j} + F)}]Hb_a\ \Delta D_a + [\sqrt{E_{v_i}(E_{v_i} + F)} - \sqrt{E_{v_j}(E_{v_j} + F)}]Hb_v\ \Delta D_v. \tag{5}$$

Note that the term ΔA_s in (4) is independent of wavelength [27] and the time difference between recording of both wavelengths is negligible compared to typical time for human motions. This term is now effectively removed in (5). Consequently, the signal portion due to blood pulsation will remain in ΔA_{ij_t} and the effect of tissue during body movement will be canceled out. As it will be discussed later, the reference signal associated with ΔA_{ij_t} will effectively be used in an adaptive filter to enhance signal quality for extracting the PPG fundamental period. Fundamental period will, therefore, be reliably extracted after signal enhancement using the generated reference signal.

B. Venous Blood Movement

Another main source of error and interference is the change of venous blood during motions. Effect of venous blood appears in calculation of oxygen saturation more noticeably, while effect of tissue hinders extraction of HR significantly. In the first step of the algorithm (see Section IV), motion artifact due to tissue effect is removed using ΔA_{ij_t} as a reference signal. This is equivalent to considering $\Delta A_s = 0$ in the second step where we

remove effect of venous blood movement. Therefore, we get the following equations for a two-wavelength PPG biosensor:

$$\begin{cases} \Delta A_i = \sqrt{E_{a_i}(E_{a_i}+F)}Hb_a\ \Delta D_a \\ \qquad\quad +\sqrt{E_{v_i}(E_{v_i}+F)}Hb_v\ \Delta D_v \\ \Delta A_j = \sqrt{E_{a_j}(E_{a_j}+F)}Hb_a\ \Delta D_a \\ \qquad\quad +\sqrt{E_{v_j}(E_{v_j}+F)}Hb_v\ \Delta D_v. \end{cases} \tag{6}$$

There are two sources of information, ΔA_i and ΔA_j, and each source is a mixture of arterial blood (represented by subscript a) and venous blood (represented by subscript v) at a particular wavelength. The first term of optical density in (6) represents the arterial signal and the second term represents the venous blood signal. We introduce weighted subtraction of these two sources, venous reference noise, $\Delta A_{ij\_v} = \Delta A_i - \beta \Delta A_j$ as

$$\begin{cases} \Delta A_{ij\_v} = \left[(r_a-\beta)\sqrt{E_{a_j}(E_{a_j}+F)}\right] Hb_a\ \Delta D_a \\ \qquad\quad +\left[(r_v-\beta)\sqrt{E_{v_j}(E_{v_j}+F)}\right] Hb_v\ \Delta D_v \\ r_a = \sqrt{E_{a_i}(E_{a_i}+F)}/\sqrt{E_{a_j}(E_{a_j}+F)} \\ r_v = \sqrt{E_{v_i}(E_{v_i}+F)}/\sqrt{E_{v_j}(E_{v_j}+F)} \end{cases} \tag{7}$$

where r_a is the ratio of arterial optical densities which is linearly related to arterial oxygen saturation and r_v is the ratio of venous optical densities. After removal of the tissue effect, the weighted subtraction of optical densities can be used to separate two signal sources related to artery and venous. Equation (7) implies that with proper tuning of β, signal associated with ΔA_{ij_v} may contain venous source (i.e., $\beta = r_a$), artery source (i.e., $\beta = r_v$) or a combination of these two sources. In other words, we can sweep β and generate a reference signal for the various values of β. There is always a range of β where the reference signal has the venous component and a wider range where the output signal has the arterial component.

Successful separation of the venous component in (7) allows us to use it as the reference noise signal in an adaptive filter to remove the venous noise from (6). In order to find β that removes arterial signal [first term of (7)] and keeps venous signal, we need a criteria to quantify the performance of any given β. The arterial signal is a periodic signal with a temporal structure. The more pronounced periodic property of the arterial term in (7) will be exploited by the subsequent adaptive and prediction error filtering to separate these two signals leading us to obtain good estimate of the arterial signal. In the next section, we formulate this problem to find the optimum β ($\beta_{\rm opt}$) to be used in estimating the venous noise reference signal and to implement an adaptive filter for removal of venous blood movement noise.

C. Optimum β

To explain the algorithm for optimum β, model of Fig. 3(a) is developed. This model consists of three main units: weighted subtracter, adaptive enhancer, and predictor filter. The adaptive enhancer is added to remove the second term of ΔA_i in (6) and keep the arterial component using the subtracter output as the reference noise. The prediction error filtering is used to predict

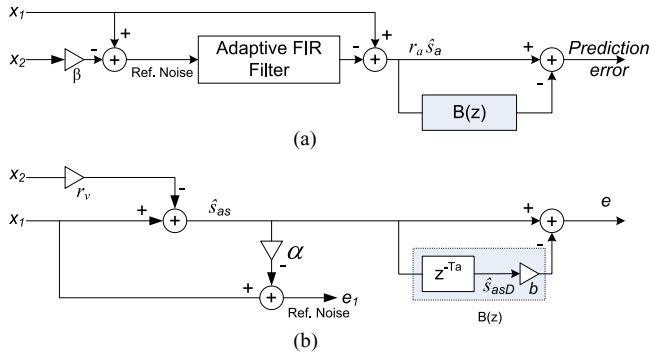

Fig. 3. Modeling temporal structure using predictor filter.

the arterial component using previous values of the signal and generate the prediction error.

Inputs x_1 and x_2 corresponding to the optical densities ΔA_i and ΔA_j in (6) are linear combinations of arterial and venous signals. Using arterial and venous optical density ratios, r_a and r_v, defined in (7), x_1 and x_2 can be expressed as

$$\begin{cases} x_1 = r_a s_a + r_v s_v \\ x_2 = s_a + s_v. \end{cases} \tag{8}$$

The subtracter generates weighted subtraction of input signals x_1 and x_2 and generates a noise reference signal corresponding to ΔA_{ij_v} in (7). The adaptive filter uses this noise reference signal to filter out the noise, second term of (6). Arterial source signal is a temporally correlated signal. As shown in Fig. 3(a), the temporal structure of the enhanced arterial signal can be modeled with an adaptive filter with the z-transform of $B(z)$ at the output of the adaptive enhancer. The predictor filter models the generated arterial signal, $r_a\hat{s}_a(n)$. The role of $B(z)$ is to estimate $r_a\hat{s}_a$ for any given β. For the optimum value of $\beta, r_a\hat{s}_a \approx \sqrt{E_{a_i}(E_{a_i}+F)}Hb\ \Delta D_a$ (i.e., the first term of ΔA_i), which is a predictable (periodic) signal representing arterial signal. Therefore, for $\beta_{\rm opt}$, the variance of the prediction error will be minimized.

In order to find optimum β, algorithm of Fig. 3(b) is implemented. This algorithm first extracts a scaled estimate of the arterial signal in x_1 (i.e. $\hat{s}_{as}$) by minimizing variance of the error signal $e(n)$ at the output of the linear predictor. The error signal, e, is the difference between current sample of $\hat{s}_{as}(n)$ and the output of the linear predictor filter $B(z)$ which can be a simple finite impulse response (FIR) filter. This relation can be mathematically expressed as

$$e(n) = (1 - B(z))\hat{s}_{as}(n). \tag{9}$$

Generally, the FIR prediction filter of order P can be expressed as

$$B(z) = \sum_{l=0}^{P} b_l z^{-l}. \tag{10}$$

Optimization of r_v and coefficient of $B(z)$ can be done by minimizing mean square error defined as the cost function:

$$J(r_v, \mathbf{b}) = E[e^2] \tag{11}$$

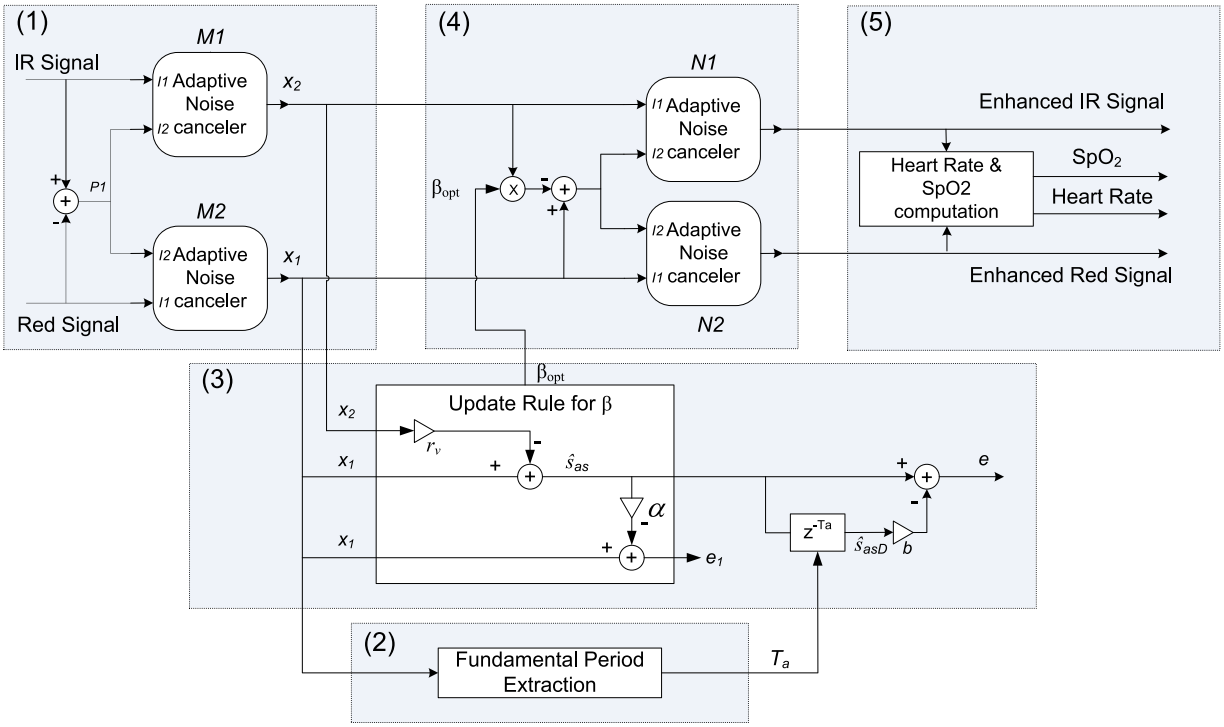

Fig. 4. Proposed motion-tolerant algorithm for signal enhancement.

where $\mathbf{b}$ is the vector of coefficient of FIR filter. This cost function has been previously used in the context of blind signal extraction [28]. In order to simplify the computation and use the extracted fundamental period of the signal, a linear predictor is chosen, $B(z) = bz^{-T_a}$, where T_a is the fundamental period of the arterial source signal in discrete time and b is the only coefficient of the filter. The cost function, $E[e^2]$, can be manipulated and written as

$$J(r_v, b) = E[\hat{s}_{as}^2(n)] - 2bE[\hat{s}_{as}(n)\hat{s}_{as}(n - T_a)] + b^2 E[\hat{s}_{as}^2(n - T_a)]. \quad (12)$$

When the gradients of the cost function with respect to r_v and b are zero, the prediction error has its minimum value. So, by equating gradient of the cost function with respect to r_v and b to zero, we obtain a system of equations. Solving this system of equations, we have

$$r_v = \frac{-E[x_1^2]E[\hat{s}_{asD}x_2] + E[x_1x_2]E[\hat{s}_{asD}x_1]}{E[x_2^2]E[\hat{s}_{asD}x_1] - E[x_1x_2]E[\hat{s}_{asD}x_2]} \quad (13)$$

and

$$b = E[\hat{s}_{as}(n)\hat{s}_{as}(n - T_a)]/E[\hat{s}_{as}^2(n - T_a)]. \quad (14)$$

It can be proven that for every given b, including b for which $\frac{\partial J(r_v,b)}{\partial r_v} = 0$, the error curve is a quadratic function of r_v and there is always a single minimum on the error curve. After extraction of the scaled estimate of the arterial signal (i.e., $\hat{s}_{as}$) in x_1, the reference noise is extracted by removing estimate of arterial signal from x_1. This is done by minimizing variance of signal e_1 (reference noise) in Fig. 3(b). By taking gradient of $E[e_1^2]$ with respect to α, we obtain

$$\alpha = \frac{E[x_1^2] - r_v E[x_1x_2]}{E[\hat{s}_{as}]}. \quad (15)$$

Signal e_1 in Fig. 3(b) is actually the reference noise. Therefore, linear combination of signals x_1 and x_2 (i.e., $x_1 - \beta x_2$) with optimum $\beta, \beta_{\text{opt}} = \frac{\alpha r_v}{1-\alpha}$, in Fig. 3(b) provides an estimate of the reference venous noise source.

IV. Proposed Noise-Tolerant Algorithm

The proposed algorithm for signal enhancement and extraction of SpO_2/HR is shown in Fig. 4. Our adaptive algorithm has five main steps:

1) Remove motion noise due to tissue effect from red and infrared signals.
2) Extract fundamental period using enhanced red or infrared signals of step 1.
3) Find optimum venous noise reference (i.e., finding β_{opt}) using red or infrared signals of step 1.
4) Enhance red and infrared signals using time-variant β_{opt} for monitoring and further feature extraction.
5) Calculate HR and SpO_2 using signal obtained after removal of motion noise due to tissue and venous blood changes during bodily movement.

Next, we explain each of the aforementioned steps implemented in block diagram of Fig. 4.

A. Tissue Effect

As we discussed in Section III, by subtracting the red and infrared signals, a reference signal is obtained (i.e., point P1

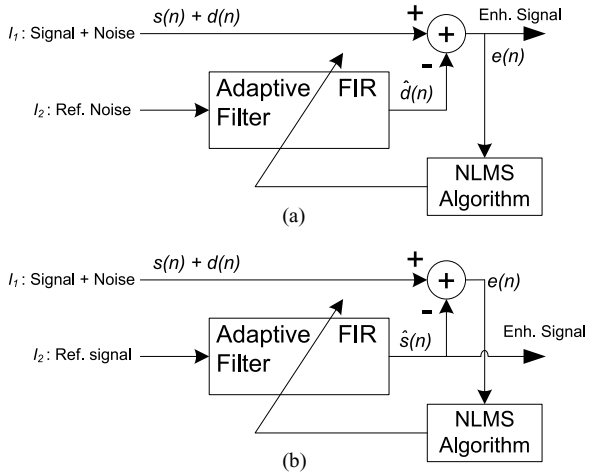

Fig. 5. Adaptive noise canceler (a) with reference noise (N) and (b) with reference signal (M).

in Fig. 4) which corresponds to ΔA_{ij_t} in (5). This reference signal is used in adaptive filters ($M1$ and $M2$ blocks in Fig. 4) to enhance the red and infrared signals, respectively. As shown in Fig. 5, adaptive noise canceler basically consists of a *filtering process* which applies a linear filter on a reference input. For instance, the reference signal I_2 in Fig. 5(a) is linearly correlated with $d(n)$, the noise component in I_1. Hence, by subtracting the filter output, $\hat{d}(n)$, from a desired response, $s(n) + d(n)$ an estimation error will be generated. An *adaptive process* automatically updates the coefficient of the filter based on a criteria extracted from the estimation error. This criteria will be defined by the adaptive algorithm used for automatic update of the coefficients. One of the most commonly used algorithms is the least mean square algorithm and its variations. The adaptive algorithm used in this study is the normalized least mean square (NLMS) algorithm due to its lower complexity compared with other techniques and immunity to the fluctuation in the signal energy.

Given the desired signal, input reference signal I_2, and the current value of the filter coefficient $\mathbf{w}(n)$, the update equation can be expresses as

$$\mathbf{w}(n+1) = \mathbf{w}(n) + \frac{2\eta}{\varepsilon + \sum_{i=0}^{N-1} I_2^2(n-i)} \mathbf{I_2}(n) e(n) \quad (16)$$

where N is the length of the adaptive filter and $0 < \eta < 1$. ε is a small number to avoid division by zero due to numerical and fixed-point computations. The error signals $e(n)$ in Fig. 5(a) and (b) are $s(n) + d(n) - \hat{d}(n)$ and $d(n) + s(n) - \hat{s}(n)$, respectively. In adaptive noise canceler of Fig. 5(a), the reference signal is only correlated with the noise source. Therefore, minimizing error power minimizes the noise power in mean square sense and enhanced signal will be obtained at the output. Similarly, in adaptive noise canceler of Fig. 5(b), the reference signal is only correlated with the signal source $s(n)$. Therefore, minimizing error power results in an enhanced noise at the primary output, but an enhanced signal output $\hat{s}(n)$ is also available. Input red and infrared signals corrupted by motion noise are

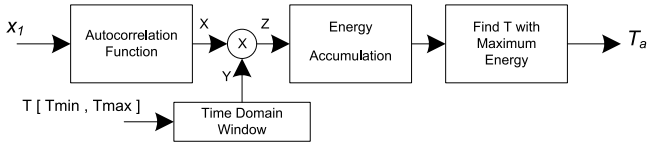

Fig. 6. Real-time fundamental period estimator.

desired signals in filters $M1$ and $M2$ [i.e., input I_1 in Fig. 5(b)]. The reference signal in filters $M1$ and $M2$ of Fig. 4 represent the true signal. The enhanced output x_1 and x_2 in Fig. 4 are red and infrared signal after the removal of tissue effect coming from enhanced signal output in Fig. 5(b).

B. Fundamental Period Extraction

The autocorrelation function $C(t)$ preserves periodicity information of the input signal. When N samples of signal are available, autocorrelation can be expressed as

$$C(t) = \frac{1}{N} \sum_{n=0}^{N-1} x_1(n) x_1(n+t) \quad (17)$$

for N larger than period of $C(t), T_a$, where $x_1(n)$ denotes PPG signal at the adaptive noise canceler $M2$ in Fig. 4, t is a lag value, and n is discrete time. Both n and t are integers representing time indices. The autocorrelation sequence has its maximum value at lag zero and integer multiples of its fundamental period, T_a.

The autocorrelation-based method used for pitch detection in speech signals [29] works well in the presence of additive noise. Adopting and tuning this technique from speech processing, we have developed a fundamental period estimator for PPG biosensors shown in Fig. 6. It is assumed that the period stays the same, i.e., the signal is stationary on each frame. The three key steps involved in this technique are as follows.

1) The autocorrelation of PPG signal is computed, i.e., point X in Fig. 6 (Window length of autocorrelation function is 1500 samples).
2) For each T in the limited range of the period, a window, $\alpha_1\delta(t-T) + \alpha_2\delta(t-2T) + \alpha_3\delta(t-3T)$, is generated (i.e., point Y in Fig. 6). Windows are multiplied with autocorrelation function in time domain. This step results in a modified autocorrelation function for each window in point Z of Fig. 6 which is zero for all T's except $T, 2T$, and $3T$.
3) For all modified autocorrelations of step 2, summation of the autocorrelation function is computed and the window passing maximum energy defines period and hence fundamental period, T_a.

α_1, α_2, and α_3 are empirically obtained as 1, 0.9, and 0.8, respectively, to enhance the accuracy of period estimator and prevent gross errors. The decreasing amplitude of window is considered to reduce susceptibility to period doubling. The extracted fundamental period, T_a, is used in prediction error filter to find the optimum β.

C. Updating Optimum β

After removing motion noise due to tissue effect and extracting fundamental period, T_a, two signals x_1 and x_2 in Fig. 4 associated with ΔA_i and ΔA_j are ready. Weighted subtraction of these two signals with current $\beta_{\rm opt}$ is used to form (7) as a reference noise for adaptive filters N1 and N2 in Fig. 4. Extracted fundamental period is used in the linear predictor to generate prediction error, e. The optimum β is updated using update rules (13) and (15) for r_v and α, respectively. This process is done on a frame basis, and for each frame a new $\beta_{\rm opt}$ is extracted. $\beta_{\rm opt}$ gives us the best noise reference, and consequently, the enhanced output signals contain only arterial component needed to extract features such as $\rm SpO_2$.

D. Signal Enhancement

The time-variant $\beta_{\rm opt}$ that provides the best estimation of motion noise due to venous blood change is used to generate a synthetic noise reference signal, the input I_2, in adaptive filters $N1$ and $N2$ of Fig. 4. Since noise reference is provided for adaptive noise cancelers $N1$ and $N2$, adaptive noise canceler of Fig. 5(a) is used. The enhanced red and infrared signals can be used for further feature extraction and monitoring purposes. Dominant and high-power motion noise conceal the waveform amplitude of arterial component when no enhancement algorithm is applied. The proposed technique provides clean signals at the output preserving peak-to-peak value of the arterial signal for amplitude analysis.

E. SpO_2 and HR Extraction

One of the frequently used techniques for the measurement of $\rm SpO_2$ in pulse oximetry is the *ratio of ratios* technique [23], [25]. This technique extracts the dc and ac parts of the red and IR PPG signals and computes the ratio of ratios, *R*, as

$$R = \frac{R_{\rm ac}/R_{\rm dc}}{IR_{\rm ac}/IR_{\rm dc}} \tag{18}$$

where $R_{\rm ac}$ and $R_{\rm dc}$ denote the magnitudes of the pulsatile and the dc parts, respectively, of the PPG obtained at the red wavelength. Similarly, $IR_{\rm ac}$ and $IR_{\rm dc}$ are the magnitudes of the pulsatile and dc portions of the IR PPG, respectively. $\rm SpO_2$ is then calculated by employing the following empirical equation [18], [25]:

$$\rm SpO_2\% = (K_1 + K_2 R)\% \tag{19}$$

where K_1 and K_2 are constants empirically found and tuned for a particular sensor platform.

In our algorithm, the fundamental period is actually the HR. Therefore, the HR is calculated using result of "Fundamental Period Extraction" unit in Fig. 4. However, once the clean signal is obtained as the result of our algorithm in Fig (4), any available HR extraction method in the literature can be applied based on the application and the need.

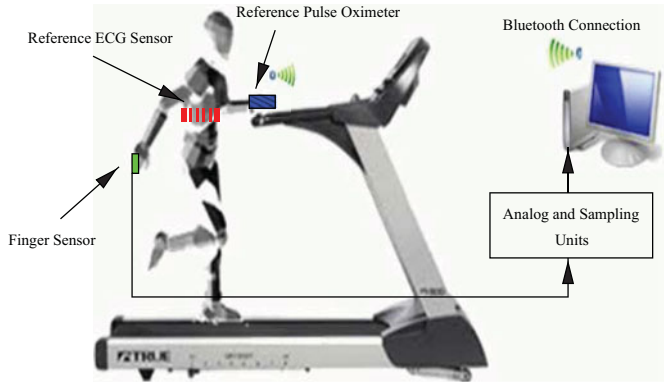

Fig. 7. Experimental setup used for data collection

V. Experimental Setup

A sensor platform is developed using a finger probe with red LED and infrared LED working at 660 and 895 nm, respectively. Analog conditioning circuit limits bandwidth of the signal to 70 Hz and it is acquired with sampling rate of 250 Hz using battery powered TMS320C5515 Evaluation Module by Texas Instrument [30]. Hamming window and a low-pass filter, with cutoff frequency at 8 Hz, are implemented on TMS320C5515 in order to attenuate the unwanted signals. The step size used for updating the filter coefficient in adaptive noise cancelers $M1$ and $M2$ of Fig. 4 is 0.002, and for both $N1$ and $N2$, the step size is 0.0008. Adaptive filters of the length 256 are used for $M1$ and $M2$ and length 1024 for $N1$ and $N2$ in Fig. 4. $K1$ and $K2$ for $\rm SpO_2$ computation [see (19)] is 105 and -23, respectively. Institutional Review Board approved and volunteers consent were obtained prior to experimentations.

For the performance evaluation, as shown in experimental setup of Fig. 7, in addition to our sensor platform, participants wore commercially available wireless ECG and $\rm SpO_2$ sensors (BioHarness BT by Zepher Technologies and Onyx II, Model 9560 by Nonin Medical Inc.). The experiment was done on a treadmill (Triumph 400T) to have control over speed and durations. To test and validate the proposed algorithm, PPG signal is collected from different subjects doing various motions. Three experimentations are designed to observe effect of motion artifact and quantify enhancement using objective and subjective tests. Fig. 8(a) shows the red PPG signal collected when the user worn the finger PPG sensor during first experiment to observe effect of motion artifact. Motion types in this test are standing, up-down, and left-right motions of the hand with different speed and acceleration, bending of the finger, walking, and running at different speeds. Six subjects between ages of 19–50 participated in the experimentation. For the objective test, an experimentation was designed to validate the performance of the algorithm during normal physical activities (standing, walking, and running). One participant, male 28 years old, did a 30-min exercise test. This exercise consisted of 5 min walking at 1 m/h, 5 min walking at 2 m/h, 5 min walking at 3 m/h, 5 min running at 4 m/h, 5 min running at 5 m/h, and then a 5 min cool down. The cool down included 1 min running at 4 m/h, 1 min walking at 3 m/h, 1 min walking at 2 m/h, and 1 min standing

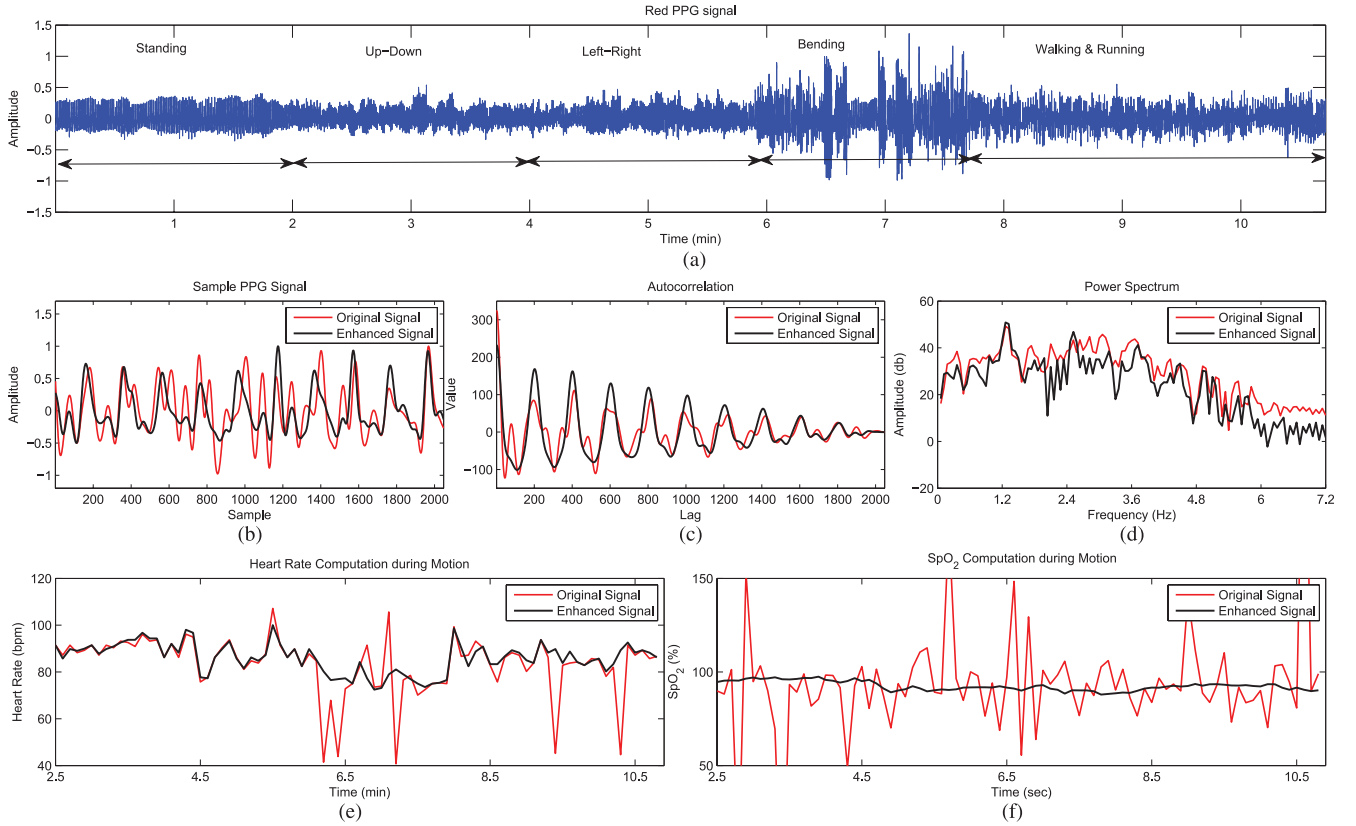

Fig. 8. (a) Sample red PPG signal collected using our sensor system during different motion types and comparing original and enhanced signals. (b) Time domain. (c) Autocorrelation. (d) Power spectrum. (e) HR. (f) SpO_2.

at rest. Six participants completed controlled subjective experiment by walking on the treadmill for 1.5 min at 2 m/h, then running at the speed of 3.5 m/h for another 1.5 min, and finally running for 2 min at 5 m/h.

VI. Experimental Results and Discussion

A. *Effect of Motion Artifact*

To see the effect of motion on the PPG signal, spectrogram of the original [see Fig. 8(a)] and enhanced PPG signal are shown in Fig. 9(a) and (b), respectively. The spectrogram is computed using short-time fourier transform with window size of 2048, overlap size of 1024 and 4096 point FFT. High-power noise component which leads to inaccurate and unreliable computation of the HR and SpO_2 can be clearly seen in the spectrogram pictured in Fig. 9(a). The removal of high-power noise components can be seen in Fig. 9(b) which leads to restoration of the true power of the signal. Harmonic enhancement can also be observed which results in enhancement of the autocorrelation function and reliable HR computation.

As an example, for the portion of the signal shown in Fig. 8(b), motion artifact has changed the shape and periodicity of the signal. Fig. 8(c) depicts autocorrelation function of the original and enhanced signal. The improvement of the autocorrelation can be observed which enables us to have a reliable HR computation.

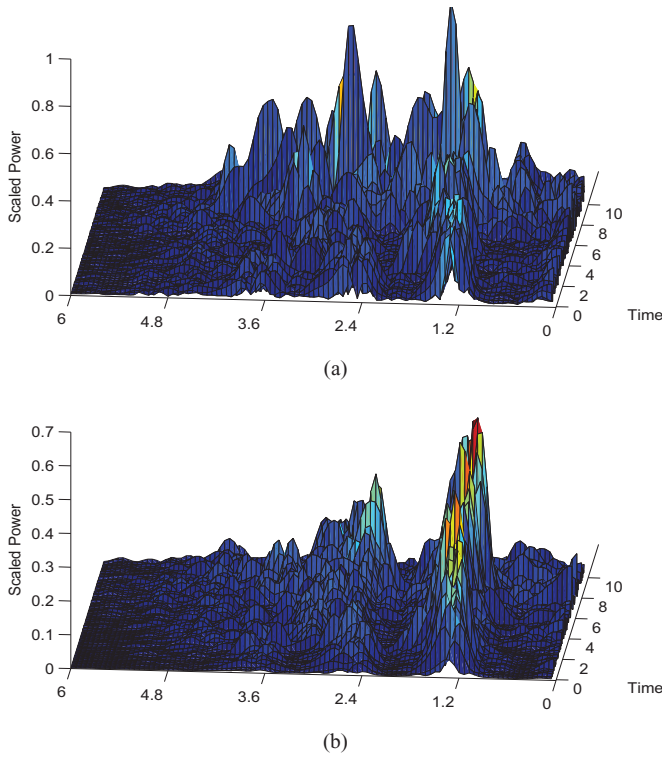

Fig. 9. Spectrogram of the PPG signal. (a) Original [see Fig. 8(a)]. (b) Enhanced.

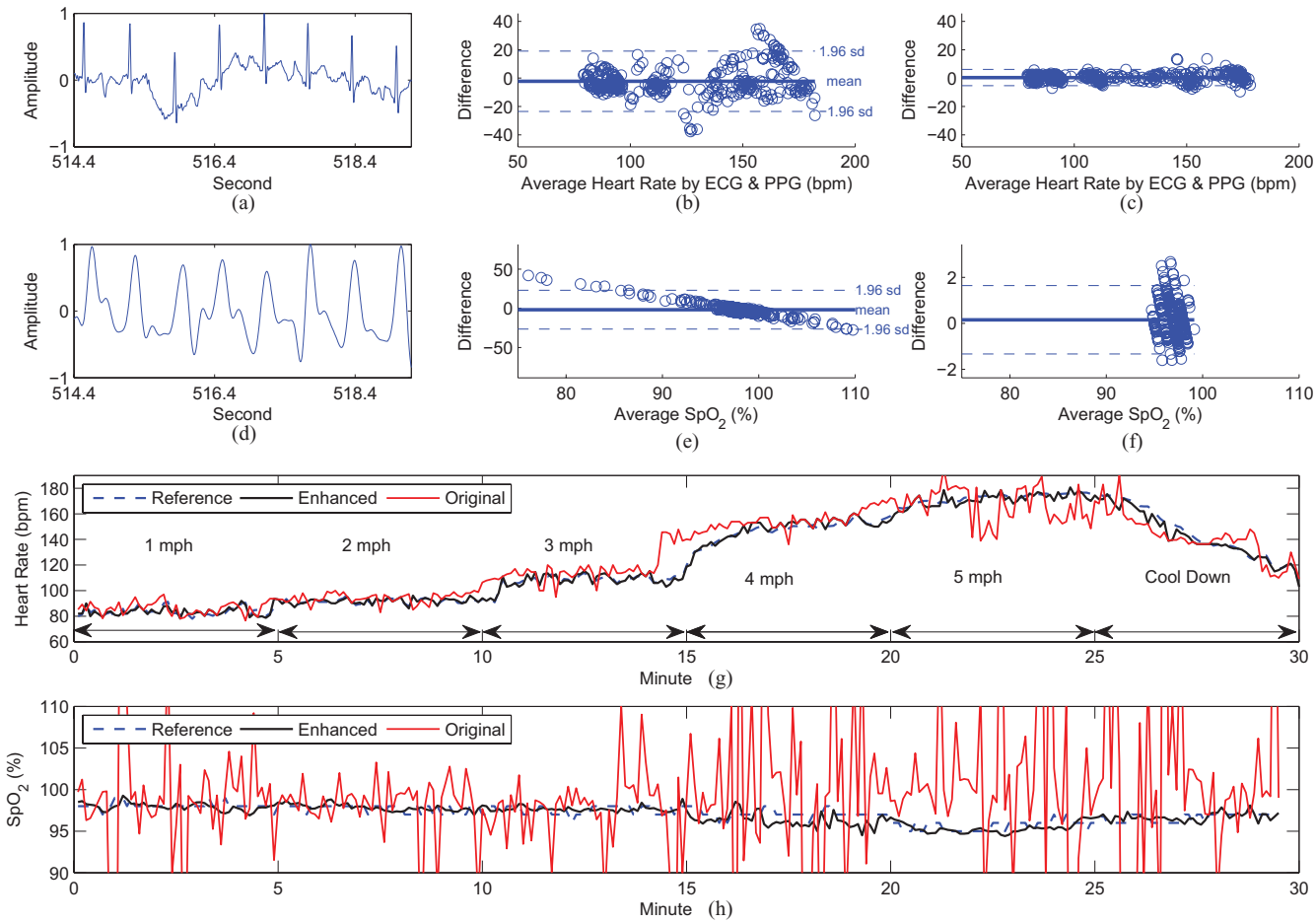

Fig. 10. (a) 5-s ECG waveform from reference ECG sensor. (b) Bland–Altman plot for original HR. (c) Bland–Altman plot for enhanced HR. (d) 5-s PPG signal from our finger sensor. (e) Bland–Altman plot for original SpO_2. (f) Bland–Altman plot for enhanced SpO_2. (g) Comparison of HR from reference ECG sensor, original signal, and enhanced signal. (h) Comparison of SpO_2 from reference oximeter, original signals, and enhanced signals.

Fig. 8(d) shows the frequency content of original and enhanced signals.

After reducing the effect of motion, HR and SpO_2 are computed every 6 s (e.g., 1500 samples) with no overlap between frames of data for original noisy signal of Fig. 8(a). The fundamental period extracted using algorithm of Fig. 6 is used for computation of the HR. Fig. 8(e) shows the HR computed using both original motion corrupted and enhanced signals (e.g., after removal of tissue effect). As seen in Fig. 8(e), after enhancing the signal, our method provides a robust HR computation. SpO_2 computation is very sensitive to the motion. Fig. 8(f) shows the SpO_2 computed using original motion corrupted signal and enhanced signal. The SpO_2 values extracted from original signal in quite unreliable, while the enhanced signal (e.g., after removal of tissue and venous effect) provides robust computation of the SpO_2.

B. Performance Evaluation, Objective, and Subjective Tests

Fig. 10(a) and (d) shows portion of ECG and PPG signals, respectively, collected using ECG sensor and our finger clip PPG sensor during objective experiment. As shown, there is a corresponding peak value for every QRS complex of ECG waveform. Bland–Altman difference plots were used to analyze the agreement between results from our algorithm and reference measurements. Limit of Agreement (LOA) in this analysis is defined as average difference ± 1.96 standard deviation of the difference ($[\mu - 1.96\sigma, \mu + 1.96\sigma]$). 95% of all differences lies inside the LOA. HR and SpO_2 values are extracted every 6 s. Three hundred pairs of HR measurement are obtained. Fig. 10(g) depicts the reference, original, and enhanced HR. Fig. 10(b) and (c) shows the agreement between HR before and after applying our algorithm. Before applying the algorithm, in many cases, the *ratio of ratios* fails to compute the SpO_2. This can be graphically seen in Fig. 10(h) in which the computed SpO_2 is shown for reference stationary sensor, original, and enhanced signal. Fig. 10(b) and (c) shows the agreement between HR computed using original and enhanced signals, respectively. Fig. 10(e) and (f) shows the Bland–Altman plot for SpO_2 computed using original and enhanced signals, respectively.

Correlation coefficient is defined as the covariance of the variables divided by their standard deviations. Correlation and agreement analyses are compared in Table I. Much higher correlation and agreement are achieved after applying our algorithm on the raw signal for SpO_2 and HR. Correlation coefficient of SpO_2 measurement after applying our algorithm was 0.71 with

TABLE I
COMPARISON OF HR AND SpO_2 ACHIEVED BEFORE AND AFTER ALGORITHM

Parameters	Corr.	Mean Bias	Mean Abs. Bias	LOA
Heart Rate (Orig.)	0.91	−2.3	8.7	[−23.5, 19.0]
Heart Rate (Enh.)	0.99	0.36	2.1	[−5.3, 6.0]
SpO_2 (Orig./Eqn. (19))	0	−1.8	6.9	[−26.5, 23.0]
SpO_2 (Orig./DST)	0.1	−5.3	25.6	[−54.3, 43.9]
SpO_2 (Enh.)	0.73	0.15	0.6	[−1.3, 1.6]

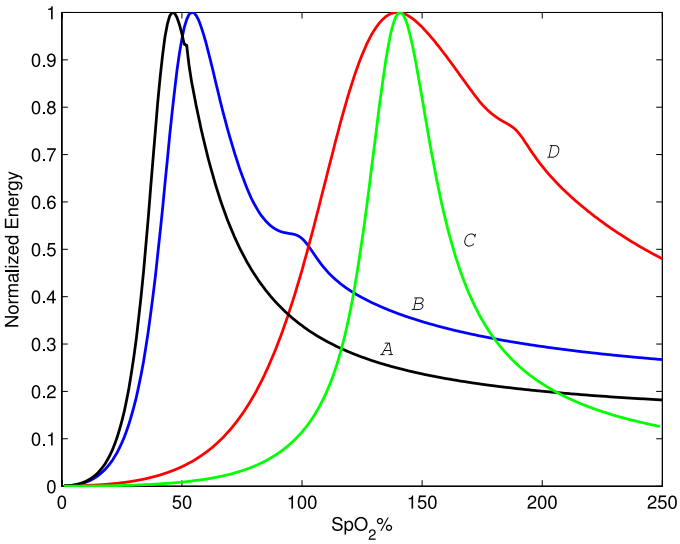

Fig. 11. Power plot of DST in the presence of motion artifact. (A) No arterial peak. (B) Arterial peak is small. (C) Increasing function with no arterial peak. (D) Increasing function with an out-of-range arterial peak.

p-value, probability of getting a correlation as large as the one obtained randomly, less than 0.00001. There is no correlation between SpO_2 computed before applying the algorithm due to high-power noise component in the signal.

For the purpose of comparison, the DST algorithm is also implemented using an adaptive filter of order 32. Reference signals are generated by sweeping SpO_2 with step size of 0.01 from 0% to 100%. SpO_2 is computed by finding the right-most peak of the power plot and results are summarized in Table I. There is a low correlation between DST algorithm and the reference SpO_2 measurements. Our proposed approach provides a more reliable SpO_2 reading with higher correlation. Fig. 11 shows some of common errors in our experimentation where the DST algorithm reports a false reading due to motion artifact. To observe the behavior of the output power plot, SpO_2 is intentionally swept in a larger range. The algorithm expects multiple peaks in the range of 0–100% where the assumption is that the right-most peak corresponds to arterial oxygen saturation. The amplitude of the peak associated with arterial oxygen saturation is typically very small as shown in power plot B in Fig. 11. These peaks can easily be affected and concealed by motion artifact as shown in power plots A and B of Fig. 11 where there is no peak related to arterial oxygen saturation on curve A. In power plots C and D, not only the peaks are affected by motion artifact but also the power curves are an increasing functions of SpO_2 in the range 0–100%. To compare our algorithm versus DST

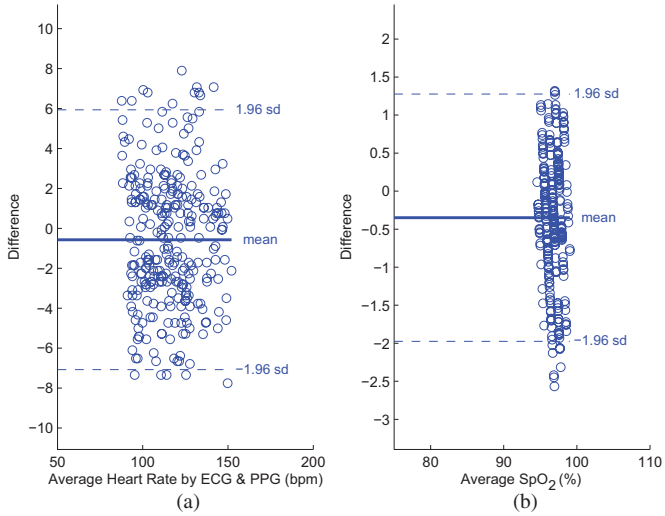

Fig. 12. Bland–Altman plots of HR and SpO_2

TABLE II
EVALUATION ON MULTISUBJECT EXPERIMENT

Parameters	Corr.	Mean Bias	Mean Abs. Bias	LOA
Heart Rate	0.98	−0.57	2.7	[−7.0, 5.9]
SpO_2	0.7	−0.35	0.71	[−1.9, 1.2]

more specifically, we computed the correlation coefficient for various levels of motions, i.e., [1 m/h, 3 m/h, 5 m/h]. The correlation coefficients for our algorithm were [0.85, 0.78, 0.64] and for DST became [0.52, 0.09, 0.03], respectively. As expected, our algorithm performs much better than DST for high level of motion artifact.

Bland–Altman plots of Fig. 12(a) and (b) show results of subjective experiment for HR and SpO_2 measurements. A total of 300 HR measurement pairs and 295 valid SpO_2 readings are computed after enhancement of the red and infrared signals. Results of this experimentation are summarized in Table II. These results for multisubject experiment overall show high level of agreement and correlation between reference measurement and our algorithm.

C. Discussion on Special Cases and Limitations

In some application such as abnormal heart rhythms and large Respiratory Sinus Arrhythmias (RSA), rapid changes in HR occur. For instance, RSA can modulate RR interval by 40–50% over a respiratory cycle [31]. In the proposed algorithm, the fundamental period is extracted using an autocorrelation-based method after removal of tissue effect. The autocorrelation-based method may result in a limited estimation error of fundamental period in such applications when compared with beat-to-beat HR. Also, batch algorithm derived for removal of venous component works on consecutive blocks of data with finite number of samples to optimize the reference noise. These sources of error might temporarily reduce quality of reference noise and consequently the filtering in the second stage. There are no such effects on the first stage of the algorithm where tissue effect

TABLE III
BEAT-TO-BEAT HR

Parameters	Error	Corr.	Mean Bias	Mean Abs. Bias	LOA
Orig. Clean BP	0.021	0.99	0	1.12	[−4.28, 4.28]
Noisy BP Signal	0.49	0.78	0.10	8.22	[−21.12, 21.24]
Enh. BP Signal	0.024	0.98	0	1.32	[−4.59, 4.59]

is removed. In order to observe sensitivity of filtering to rapid changes of HR, we have extracted beat-to-beat HR after enhancing the noisy signal with second stage of the algorithm while using autocorrelation-based fundamental period extractor and update rule for $\beta_{\rm opt}$.

Due to high similarity of BP signal with PPG signal, we have used BP signal from the MIT-BIH polysomnographic [32] database (slp01a) to evaluate beat-to-beat HR. This database includes BP and ECG signals. For evaluation purpose, reference HR is derived from annotated ECG signal in database. BP signal is standardized to have zero mean and unity variance. Noise is artificially added to 1 h of clean BP signal and signals x_1 and x_2 are generated according to (8) with $r_a = 0.9$ and $r_v = 0.6$ [typical optical density ratios in artery and vein; see also (7)]. The noise $\mathcal{N}(0, 1)$ is filtered with an FIR low-pass filter with cutoff frequency of 8 Hz and multiplied by a gain factor to have unity variance in x_1.

To extract the beat-to-beat HR from BP signal, a threshold-based method is used which finds maximum point on the signal in each cycle. BP signal is converted to frames of size 700 samples. For each new frame, the mean value is subtracted from signal and a clipping level is extracted by computing a fixed percentage of the maximum amplitude of the signal in that frame. The center clipped signal, the original signal minus the clipping level, is extracted and a peak finder finds the location of the peak value on center clipped waveform. Result are summarized in Table III. The relative *Error* in Table III is used in [33] for quantifying beat-to-beat HR and defined as

$$Error = \sqrt{\frac{1}{N}\sum_{j=1}^{N}\left[\frac{HR(j) - Ref(j)}{Ref(j)}\right]^2} \qquad (20)$$

where N is the total number of beats, and HR and Ref are measured HR and the reference HR obtained from annotated ECG signal in database, respectively. Our simulation on MIT-BIH database shows that beat-to-beat HR can reliably be extracted using our algorithm even though there is an estimation error in fundamental period due to rapid changes of the HR. Due to rapid changes in HR and high power of added noise, the threshold-based method has poor performance in extracting HR from noisy BP signal even though threshold is adaptively adjusted to have the best result. There is a high correlation between beat-to-beat HR from enhanced signal and reference beat-to-beat HR. To further reduce the effect of rhythm irregularities on reference noise in special applications, the algorithm can be tuned appropriately based on features that are supposed to be extracted from the enhanced output signals for that particular application. For instance, the size of autocorrelation window can be tuned based on the rate of changes of heart beat or it can be replaced with available reliable beat-to-beat HR extractor. As an example, Barros and Ohnishi [33] used RSA as a frequency modulation occurring on the signal. This study proposed heart instantaneous frequency with highly accurate estimation of the beat-to-beat HR. More complex prediction filter with higher order and adaptability can also be deployed to reduce impact of rhythm irregularities.

VII. CONCLUSION

In this paper, a novel adaptive algorithm was developed for signal enhancement against motion artifact. The algorithm is then used for robust extraction of HR and oxygen saturation in wearable and portable PPG biosensors. We considered different sources of error during body movement from optical theories describing pulse oximetry optics. The problem was mathematically formulated, and at each stage of enhancement, a reference signal was generated and utilized in NLMS adaptive filter. The experimental results validated reliable extraction of HR and oxygen saturation with correlation of more than 0.98 and 0.7, respectively, compared to reference stationary sensors in the presence of the motion artifact.

REFERENCES

[1] K. H. Shelley, "Photoplethysmography: Beyond the calculation of arterial oxygen saturation and heart rate," *Anesth. Analg.*, vol. 105, no. 6, pp. S31–S36, Dec. 2007.
[2] J. C. Dorlas and J. A. Nijboer, "Photo-electric plethysmography as a monitoring device in anaesthesia. Application and interpretation," *Br. J. Anaesth.*, vol. 57, pp. 524–530, 1985.
[3] V. F. Blanc, M. Haig, M. Troli, and B. Sauve, "Computerized photoplethysmography of the finger," *Can. J. Anaesth.*, vol. 40, pp. 271–278, 1993.
[4] A. Awad, M. A. Ghobashy, R. G. Stout, D. G. Silverman, and K. H. Shelley, "How does the plethysmogram derived from the pulse oximeter relate to arterial blood pressure in coronary artery bypass graft patients?," *Anesth. Analg.*, vol. 93, pp. 1466–1471, 2001.
[5] B. Jonsson, C. Laurent, T. Skau, and L. G. Lindberg, "A new probe for ankle systolic pressure measurement using photoplethysmography (PPG)," *Ann. Biomed. Engl.*, vol. 33, pp. 232–239, 2005.
[6] P. A. Leonard, J. G. Douglas, N. R. Grubb, D. Clifton, P. S. Addison, and J. N. Watson, "A fully automated algorithm for the determination of respiratory rate from the photoplethysmogram," *J. Clin. Monit. Comput.*, vol. 20, pp. 33–36, 2006.
[7] L. Nilsson, A. Johansson, and S. Kalman, "Respiration can be monitored by photoplethysmography with high sensitivity and specificity regardless of anaesthesia and ventilatory mode," *Acta Anaesth. Scand.*, vol. 49, pp. 1157–1162, 2005.
[8] J. Y. Foo and S. J. Wilson, "Estimation of breathing interval from the photoplethysmographic signals in children," *Physiol. Meas.*, vol. 26, no. 6, pp. 1049–1058, 2005.
[9] P. Bonato, D. De Rossi, A. Dittmar, S. Jayaraman, I. Korhonen, A. Lymberis, E. Mc Adams, and Y. Zhang, "IEEE EMBS technical committee on wearable biomedical sensors and systems: Position paper," in *Proc. Int. Workshop Wearable Implantable Body Sensor Netw.*, 2006, pp. 212–214.
[10] H. H. Asada, P. Shaltis, A. Reisner, S. Rhee, and R. C. Hutchinson, "Mobile monitoring with wearable photoplethysmographic biosensors," *IEEE Eng. Med. Biol. Mag.*, vol. 22, no. 3, pp. 28–40, May/Jun. 2003.
[11] R. T. Brouillette, J. Lavergne, A. Leimanis, G. M. Nixon, S. Ladan, and C. D. McGregor, "Differences in pulse oximetry technology can affect detection of sleep-disordered breathing in children," *Anesth. Analg.*, vol. 94, pp. 47–53, 2002.
[12] C. G. Durbin and S. K. Rostow, "More reliable oximetry reduces the frequency of arterial blood gas analyses and hastens oxygen weaning after cardiac surgery: A prospective, randomized trial of the clinical impact of a new technology," *Crit. Care Med.*, vol. 30, pp. 1735–1740, 2002.

[13] B. Bohnhorst and C. F. Poets, "Major reduction in alarm frequency with a new pulse oximeter," *Intens. Care Med.*, vol. 24, pp. 277–278, 1998.
[14] L. B. Wood and H. Asada, "Low variance adaptive filter for cancelling motion artifact in wearable photoplethysmogram sensor signals," in *Proc. Conf. IEEE Eng. Med. Biol. Soc.*, Aug. 2007, pp. 652–655.
[15] S. H. Kim, D. W. Ryoo, and C. Bae, "Adaptive noise cancellation using accelerometers for the PPG signal from forehead," in *Proc. Conf. IEEE Eng. Med. Biol. Soc.*, Aug. 2007, pp. 2564–2567.
[16] H. Han, M. J. Kim, and J. Kim, "Development of real-time motion artifact reduction algorithm for a wearable photoplethysmography," in *Proc. Conf. IEEE Eng. Med. Biol. Soc.*, Aug. 2007, pp. 1538–1541.
[17] H. H. Asada, H. Jiang, and P. Gibbs, "Active noise cancellation using MEMS accelerometers for motion-tolerant wearable bio-sensors," in *Proc. Conf. IEEE. Eng. Med. Biol. Soc.*, Sep. 2004, vol. 1, pp. 2157–2160.
[18] M. R. Ram, K. V. Madhav, E. H. Krishna, N. R. Komalla, and K. A. Reddy, "A Novel approach for motion artifact reduction in PPG signals based on AS-LMS adaptive filter," *IEEE Trans. Instrum. Meas.*, vol. 61, no. 5, pp. 1445–1457, May 2012.
[19] J. M. Goldman, M. T. Petterson, R. J. Kopotic, and S. J. Barker, "Masimo signal extraction pulse oximetry," *J. Clin. Monit.*, vol. 16, pp. 475–483, 2000.
[20] J. M. Graybeal and M. T. Petterson, "Adaptive filtering and alternative calculations revolutionizes pulse oximetry sensitivity and specificity during motion and low perfusion," in *Proc. IEEE Eng. Med. Biol. Soc.*, 2004, vol. 7, pp. 5363–5366.
[21] Masimo Corp. (2012). Signal extraction technology. [Online]. Available: http://www.masimo.com/pdf/whitepaper/LAB1035R.PDF
[22] R. Yousefi, M. Nourani, and I. Panahi, "Adaptive cancellation of motion artifact in wearable biosensors," in *Proc. Int. Conf. IEEE Eng. Med. Biol. Soc.*, Aug. 2012, pp. 2004–2008.
[23] J. E. Sinex, "Pulse oximetry: Principles and limitations," *Amer. J. Emerg. Med.*, vol. 17, no. 1, pp. 59–68, Jan. 1999.
[24] K. A. Reddy, B. George, N. M. Mohan, and V. J. Kumar, "A novel calibration-free method of measurement of oxygen saturation in arterial blood," *IEEE Trans. Instrum. Meas.*, vol. 58, no. 5, pp. 1699–1705, May 2009.
[25] J. G. Webster, *Design of Pulse Oximeters*. New York, NY, USA: Taylor & Francis, 1997.
[26] T. Aoyagi, M. Fuse, N. Kobayashi, K. Machida, and K. Miyasaka, "Multiwavelength pulse oximetry: Theory for the future," *Anesth. Analg.*, vol. 105, no. 6, pp. S53–S58, Dec. 2007.
[27] T. Aoyagi, "Pulse oximetry: Its invention, theory, and future," *J. Anesth.*, vol. 17, pp. 259–266, 2003.
[28] A. K. Barros and A. Cichocki, "Extraction of specific signals with temporal structure," *Neural Comput.*, vol. 13, no. 9, pp. 1995–2003, 2001.
[29] J. D. Wise, J. R. Caprio, and T. W. Parks, "Maximum likelihood pitch estimation," *IEEE Trans. Acoust. Speech Signal Process.*, vol. 24, no. 5, pp. 418–423, Oct. 1976.
[30] Texas Instrument Inc. (2013). [Online]. Available: http://www.ti.com/tool/tmdxevm5515
[31] J. A. Hirsch and B. Bishop, "Respiratory sinus arrhythmia in humans: How breathing pattern modulates heart rate," *Amer. J. Physiol.*, vol. 241, no. 4, pp. 620–629, 1981.
[32] MIT-BIH Arrhythmia Database. (2013). [Online]. Available: www.physionet.org/physiobank/database/mitdb
[33] A. K. Barros and N. Ohnishi, "Heart instantaneous frequency (HIF): An alternative approach to extract heart rate variability," *IEEE Trans. Biomed. Eng.*, vol. 48, no. 8, pp. 850–855, Aug. 2001.

Rasoul Yousefi (S'11) received the B.S. degree in electrical engineering from Shiraz University, Shiraz, Iran, and the M.Sc. degree in circuits and systems from the University of Tehran, Tehran, Iran, in 2006 and 2009, respectively. He is currently working toward the Ph.D. degree in electrical engineering at the University of Texas at Dallas, Richardson, USA.

His research interest includes digital circuits and systems and signal processing with an emphasis on medical devices and biomedical sensors. Since 2010, he has been a member of SoC Design and Test laboratory and the QoLT laboratory, University of Texas at Dallas.

Mr. Yousefi is a student member of the IEEE Engineering in Medicine and Biology Society.

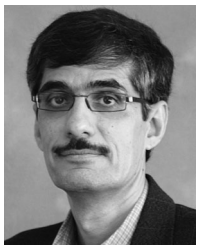

Mehrdad Nourani (S'91–M'94–SM'05) received the B.Sc. and M.Sc. degrees in electrical engineering from the University of Tehran, Tehran, Iran, and the Ph.D. degree in computer engineering from Case Western Reserve University, Cleveland, OH, USA.

He is currently a Professor of Electrical Engineering at the University of Texas at Dallas (UTD), Richardson, USA. He is a Co-Founder of the Quality of Life Technology laboratory, UTD, where he conducts an interdisciplinary research lab focused on developing innovative technology and systems that improve people's quality of life. He has published more than 250 papers in journals and refereed conference proceedings. His current research interests include fault-tolerant architectures, system-on-chip testing, design for reliability, and special-purpose IC/system design for biomedical/biological applications.

Dr. Nourani is a recipient of multiple awards from Clark Foundation Research Initiation Grant, National Science Foundation Career, Cisco Systems Inc., and Semiconductor Research Corporation. He is a member of the IEEE Computer Society and the ACM SIGDA.

Sarah Ostadabbas (S'11) received the B.Sc. degree in both electrical and biomedical engineering from Amirkabir University of Technology, Tehran, Iran, in 2005, and the M.Sc. degree in control engineering from the Sharif University of Technology, Tehran, in 2007. She is currently working toward the Ph.D. degree in electrical engineering at the University of Texas at Dallas, Richardson, USA.

Her research interests include embedded systems and signal processing with an emphasis on medical/biological applications and modeling. A major application of her research is the prevention of pressure ulcer formation and amputation through predictive modeling and scheduling therapeutic care. She is a member of the Quality of Life Technology Laboratory, University of Texas at Dallas.

Ms. Ostadabbas is a student member of the IEEE Engineering in Medicine and Biology Society and the IEEE Women in Engineering Society.

Issa Panahi (S'84–M'88–SM'07) received the M.Sc. degree in electrical engineering from Florida Institute of Technology, Melbourne, Florida, USA and the Ph.D. degree from the University of Colorado at Boulder, Colorado, USA.

He is currently an Associate Professor of Electrical Engineering and also an Associate Research Faculty of biomedical engineering at the University of Texas at Dallas (UTD), Richardson, USA. He is Founding Director of the Statistical Signal Processing and Acoustic Research Laboratories. His research interests include audio/acoustic/speech signal processing, stimation, identification, source separation, and noise cancellation. He joined the faculty of UTD after working in research centers and industry for 16 years. He was a DSP Chief Architect, Chief Technology Officer, and Advance Systems Development Manager in the embedded DSP systems business unit at Texas Instruments. He holds one US patent and is author/co-author of four Texas Instruments books and more than 80 technical journal and conference articles.

He was the Founder and Vice Chair of the IEEE-Dallas Chapter of the IEEE Engineering in Medicine and Biology Society (EMBS). He is the Chair of the IEEE Dallas Chapter of IEEE Signal Processing Society. He received the 2005 and the 2011 "Outstanding Service Award" from the IEEE Section. He was an organizing member and Chair of the Plenary Sessions of the 2010 IEEE International Conference on Acoustics, Speech, and Signal Processing. He has been session organizer and chair of several tracks at EMBS conferences.